NUMERICAL COMPUTATIONS ON FLOW AND HEAT TRANSFER OF CASSON FLUID DUE TO OSCILLATORY MOVING SURFACE

by

Sami ULLAH KHAN[a], Nasir ALI[b], Tahir MUSHTAQ[c], Amar RAUF[a], and Sabir Ali SHEHZAD[a]*

[a] Department of Mathematics, COMSATS University of Islamabad, Sahiwal, Pakistan
[b] Department of Mathematics and Statistics, International Islamic University, Islamabad, Pakistan
[c] Department of Mathematics, COMSATS University of Islamabad, Vehari, Pakistan

Original scientific paper
https://doi.org/10.2298/TSCI171130091U

A numerical study of unsteady hydromagnetic flow of Casson liquid passed through the oscillatory moving surface is presented. The interaction of radiation term is reported in the energy equation. The flow is generated by the rapid movement of elastic surface that stretched back and forth periodically. The number of variables is reduced by introducing dimensionless variables. An implicit technique developed on finite difference algorithm is implemented to the system of PDE. The impact of various parameters like Casson liquid parameter, the oscillation frequency and stretching rate ratio, Hartmann number and effective Prandtl number are shown through various graphs. The observation indicates that the amplitude of the velocity declines by enhancing Casson liquid parameter, oscillation frequency and stretching rate ratio and Hartmann number. The temperature declines by increasing Casson fluid parameter and effective Prandtl number. The results also indicate that the time-series of local Nusselt number increases by enhancing effective Prandtl number.

Key words: *Casson fluid, oscillatory moving sheet, heat transfer, finite difference technique*

Introduction

Flow behavior of non-Newtonian materials has gained much interest among the researchers owing to their practical application in industry and engineering, particularly in the polymer technology. Unlike Newtonian fluids, such flow phenomena have a complex relation between the strain rate and shear stress. Non-Newtonian fluids are encountered in chemical and nuclear plants, bioengineering and material processing, *etc*. Such fluids include polymer liquids, paper pulp, molten plastics, certain oils, foodstuff, shampoos, apple sauce, animal blood, paints, ketchup and slurries. The salient characteristics of such fluids cannot be described through a constitutive relationship. Therefore, various flow models [1-9] have been presented in past decades to analyze significance characteristics of non-Newtonian fluids.

The most important class is the Casson fluid model. Such fluid is plastic fluid that displays thinning characteristics. If yield stress is higher than the shear stress, it acts as a solid while in opposite scenario we have a moving fluid. The model is applicable for liquids containing rods as solids and also valid for blood and molten chocolate. Walawender *et al.* [10]

* Corresponding author, e-mail: ali_qau70@yahoo.com

analyzed that the constitutive equations of Casson fluid described accurately flow characteristics of pigments suspensions in the lithographic varnishes, used for the preparation of silicon suspensions and printing inks. Many researchers investigated the flow model of Casson fluid by considering various geometrical aspects. Hayat *et al.* [11] computed analytic solution to analyze the flow behavior of Casson liquid. The steady flow of Casson liquid through a stretching/shrinking sheet by shooting technique has been reported by Bhattacharyya *et al.* [12]. The effects of chemically reactive flow of Casson liquid flowing to stretching surface was analyzed by Mukhopadhyay [13]. Shehzad *et al.* [14] reported the analytical study of Casson fluid through a stretching surface considering the impact of chemical reaction. Mukhopadhyay and Mandal [15] studied the flow characteristics of Casson fluid passed through porous wedge. Mustafa and Khan [16] presented the numerical investigations for flow of Casson nanofluid. Study concerning the flow characteristics using Casson fluid model can be found in [17-20].

The MHD has vital applications in physics, chemistry, engineering and medicine. Various industrial equipment's like optical grating, fiber filters, optical switches, tunable optical filters and modulators, pumping machines, bearings, stretching of the plastic sheets and MHD generators are affected due to magnetic field and electrically conducting liquid interaction. In metallurgy the thinning and annealing of the copper wires, cooling of strips in the process of drawing are need to be stretched for the final product. The required quality in these situations strongly depends upon rate of cooling, which can be achieved by drawing the strips in an electrically conducting liquid. The occurrence of magnetic field has a significance role in controlling the momentum and transfer of heat in different types of fluid flows. The comprehensive review on magnetic field can be found in refs. [21-27].

The thermal radiations effects at high operating temperature are quite significant in the heat transfer phenomenon. It is well-accepted fact that several industrial and chemical engineering processes occurs at large temperature difference like glass fiber, gas turbines, filaments, hot rolling, solar power technology, aircrafts, nuclear plants, IC engines, propulsion devices, space vehicles and satellites. In such type of phenomenon, the importance of thermal radiation cannot be denied. The impact of thermally radiative flow of nanofluid past a curved stretching sheet was studied by Abbas *et al.* [28]. Hayat *et al.* [29] reported the analytical study of boundary-layer flow of Carreau fluid encounter the impact of radiation. The model of thermally radiative flow owing to a curved sheet was presented by Hayat *et al.* [30]. Ample attempts have been made in this regard [31-36].

Fluid flow over stretching surfaces has attract investigators in last decades because of its abundant applications in engineering point of view such as paper production, rubber sheets extrusion, artificial fibers, paper production, melt-spinning, *etc*. Many researchers devoted his time for flow problems by considering different types of surfaces. Among them the Oscillatory stretching surface is the most important one. Wang [37] initiated the fluid flow problem considering the oscillatory stretching sheet. He computed perturbation solution of the considered problem. Abbas *et al.* [38] studied the laminar flow of viscoelastic fluid owing to oscillatory stretching surface. The Wang's problem is extended by Abbas *et al.* [39] for the analysis of heat transfer in electrically conducting viscous fluid. Soret-Dufour phenomenon of unsteady viscous liquid due to oscillatory moving surface has been reported by Zheng *et al.* [40]. Ali *et al.* [41] discussed the flow of Jeffrey fluid passed through oscillatory surface. A numerical solution for laminar viscoelastic second grade fluid due to oscillatory moving surface considering the impacts of heat transfer was prescribed by Khan *et al.* [42].The hydromagnetic flow of Couple stress fluid over an oscillatory stretching sheet with absorption/generation effects was investigated by Ali *et al.* [43].

Our aim is to present a numerical analysis of unsteady radiative Casson liquid flow through oscillatory sheet due to occurrence of magnetic field. This phenomenon is not presented till now in literature.

Flow model

The problem of unsteady radiative Casson liquid flow through an oscillatory moving surface with the effect of magnetic field is reported. We choose x-axis along sheet while y is perpendicular to it. At $t > 0$, the surface is stretched and oscillates periodically, fig. 1. Let fluid maintains constant temperature T_w near the sheet and temperature T_∞ away from it. The governing equations of flow are:

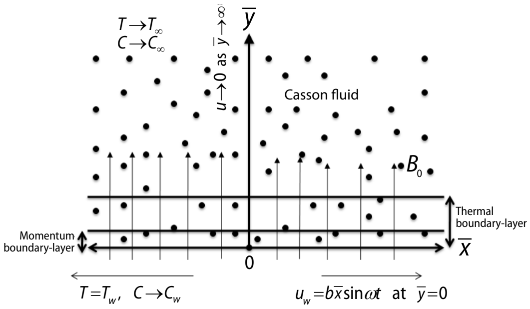

Figure 1. Geometry of problem

$$\frac{\partial u}{\partial x} + \frac{\partial v}{\partial y} = 0 \tag{1}$$

$$\frac{\partial u}{\partial t} + u\frac{\partial u}{\partial x} + v\frac{\partial u}{\partial y} = \nu\left(1 + \frac{1}{\beta}\right)\frac{\partial^2 u}{\partial y^2} - \frac{\sigma B_0^2}{\rho}u \tag{2}$$

$$\rho c_p\left(\frac{\partial T}{\partial t} + u\frac{\partial T}{\partial x} + v\frac{\partial T}{\partial y}\right) = k\frac{\partial^2 T}{\partial y^2} - \frac{\partial q_r}{\partial y} \tag{3}$$

in which we denote u and v as velocity components, ν – the kinematic viscosity, β – the Casson liquid parameter, ρ – the liquid density, B_0 – the strength of applied magnetic field, c_p – the specific heat, k – the thermal conductivity, σ – the electrical conductivity, T – the temperature, and q_r – the heat flux of radiation.

Using the Rosseland approximation [28], we have:

$$q_r = -\frac{4\sigma^*}{3k^*}\frac{\partial T^4}{\partial y} \tag{4}$$

where σ^* is the Stefan Boltzmann constant and k^* – the absorption constant. For further analysis, we assume that the temperature gradients within the flow are small. As an implication of this assumption the term T^4 appearing in eq. (4) may be linearized about the ambient temperature T_∞ using Taylor series to give:

$$T^4 = T_\infty^4 + 4T_\infty^3\left(T - T_\infty\right) + 6T_\infty^2\left(T - T_\infty\right)^2 + ... \tag{5}$$

Upon neglecting the higher-order terms, we get:

$$T^4 \cong 4TT_\infty^3 - 3T_\infty^4 \tag{6}$$

In view of eqs. (4) and (5), eq. (3) takes the form:

$$\rho c_p\left(\frac{\partial T}{\partial t} + u\frac{\partial T}{\partial x} + v\frac{\partial T}{\partial y}\right) = \left(k + \frac{16\sigma^* T_\infty^3}{3k^*}\right)\frac{\partial^2 T}{\partial y^2} \tag{7}$$

The following boundary conditions are utilized:

$$\begin{cases} u = u_w = bx\sin\omega t, \quad v = 0, \quad T = T_w \quad \text{at} \quad y = 0, \quad t > 0 \\ u \to 0, \quad T \to T_\infty \quad \text{as} \quad y \to \infty, \end{cases} \tag{8}$$

Introducing the appropriate variables [37-40]:

$$\xi = \sqrt{\frac{b}{\nu}}y, \quad \tau = t\omega, \quad u = bxf_\xi(\xi,\tau), \quad v = -\sqrt{\nu b}, f(\xi,\tau), \quad \theta(\xi,\tau) = \frac{T - T_\infty}{T_w - T_\infty}. \tag{9}$$

In view of eq. (9), we note that eq. (1) satisfied and eqs. (2) and (7) become:

$$\left(1 + \frac{1}{\beta}\right) f_{\xi\xi\xi} - Sf_{\xi\tau} - f_\xi^2 + ff_{\xi\xi} - \mathrm{M}^2 f_\xi = 0 \tag{10}$$

$$\frac{1}{\mathrm{Pr}}(1 + N_r)\theta_{\xi\xi} + f\theta_\xi - S\theta_\tau = 0 \tag{11}$$

where $S \equiv \omega/b$ is the ratio of oscillation frequency and stretching rated surface, $\mathrm{M} = (\sigma B_0^2/\rho b)^{1/2}$ – the Hartmann number, $\mathrm{Pr} = \mu c_p/k$ – the Prandtl number, and $N_r = 16\sigma^* T_\infty^3/3k^* k$ – the radiative parameter. Equation (10) become in view of [35]:

$$\frac{1}{\mathrm{Pr}_{eff}}\theta_{yy} + f\theta_y - S\theta_\tau = 0 \tag{12}$$

where $\mathrm{Pr}_{eff} = \mathrm{Pr}/(1 + N_r)$ corresponds to effective Prandtl number.

The associated boundary conditions take the following form:

$$\begin{cases} f_\zeta(0,\tau) = \sin\tau, \quad f(0,\tau) = 0, \quad \theta(0,\tau) = 1 \\ f_\zeta(\infty,\tau) \to 0, \quad \theta(\infty,\tau) \to 0 \end{cases} \tag{13}$$

The local Nusselt number in present case is:

$$\mathrm{Nu}_x = \frac{xq_w}{k(T - T_\infty)}, \quad q_w = -k\left(1 + \frac{16\sigma^* T_\infty^3}{3kk^*}\right)\left(\frac{\partial T}{\partial y}\right) \tag{14}$$

The dimensionless expression of local Nusselt number is:

$$\mathrm{Re}_x^{-1/2}\,\mathrm{Nu}_x^* = -\theta_\xi(0,\tau) \tag{15}$$

where $\mathrm{Re}_x = u_w x/\nu$ is the local Reynolds number and $\mathrm{Nu}_x^* = \mathrm{Nu}_x/(1 + N_r)$ is the effective local Nusselt number [35].

Numerical solution

In order to find the approximate solution of eqs. (10) and (12) with boundary conditions (13), a numerical based technique namely infinite difference scheme is implemented, fig. 2. First the semi-infinte domain is truncated. The approximate solution is computed by truncating the semi-infinite domain. For this purpose the semi-infinite domain $\xi \in [0,\infty)$ is transformed into finite domain $\xi \in [0,H]$ and boundary conditions at infinity $y \to \infty$ is endorsed at $\xi = H$. It is remarked that the length of H is adjusted in such a way that any other amendment in its value does not considerably alter the solution [38, 39]. In this paper co-ordinate transformation $\psi = 1/(\xi+1)$ is suggested to transform the infinite physical domain $\xi \in [0,\infty)$ into a domain $\psi \in [0,1]$:

$$\xi = \frac{1}{\psi} - 1, \quad \frac{\partial}{\partial \xi} = -\psi^2 \frac{\partial}{\partial \psi},$$
$$\frac{\partial^2}{\partial \xi^2} = \psi^4 \frac{\partial^2}{\partial \psi^2} + 2\psi^3 \frac{\partial}{\partial \psi},$$
$$\frac{\partial^2}{\partial \xi \partial \tau} = -\psi^2 \frac{\partial^2}{\partial \psi \partial \tau}$$
$$\frac{\partial^3}{\partial \xi^3} = -\psi^6 \frac{\partial^3}{\partial \psi^3} - 6\psi^5 \frac{\partial^2}{\partial \psi^2} - 6\psi^4 \frac{\partial}{\partial \psi}$$

Substituting aforementioned transformations in eqs. (10) and (12), we have:

$$S\frac{\partial^2 f}{\partial \psi \partial \tau} = \psi^2 \left(\frac{\partial f}{\partial \psi}\right)^2 - \left[6\psi^2\left(1+\frac{1}{\beta}\right) - 2\psi f - \mathrm{M}^2\right]\left(\frac{\partial f}{\partial \psi}\right) + \left[6\psi^3\left(1+\frac{1}{\beta}\right) - \psi^2 f\right]\left(\frac{\partial^2 f}{\partial \psi^2}\right) + \left(1+\frac{1}{\beta}\right)\psi^4 \frac{\partial^3 f}{\partial \psi^3} \tag{16}$$

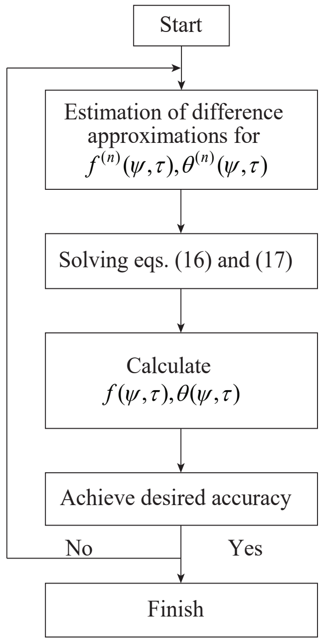

Figure 2. The flow chart of the numerical method

$$\frac{1}{\mathrm{Pr}_{eff}}\left(\psi^4 \frac{\partial^2 \theta}{\partial \psi^2} + 2\psi^3 \frac{\partial \theta}{\partial \psi}\right) - \left(f\psi^2 \frac{\partial \theta}{\partial \psi} + S\frac{\partial \theta}{\partial \tau}\right) = 0 \tag{17}$$

$$\begin{cases} f_\psi = 0, \quad \theta = 0 \quad \text{at} \quad \psi = 0 \\ f = 0, \quad f_\psi = -\sin\tau, \quad \theta = 1 \quad \text{at} \quad \psi = 1 \end{cases} \tag{18}$$

The numerical procedure is implemented in the following steps. We discretize eqs. (15)-(17) for L uniformly distributed discrete points in $\psi = (\psi_1, \psi_2, ..., \psi_L) \in (0,1)$ with a space grid size of $\Delta\psi = 1/(L+1)$ and time level $\tau = (\tau^1, \tau^2, ...) = (\Delta\tau, 2\Delta\tau, ..., n\Delta\tau, ...)$, where Δt is the time step size. Hence the discrete values $(f_1^n, f_2^n, ..., f_L^n)$ at these grid point for time levels $\tau^n = n\Delta\tau$ (Δt is the time step size) can be numerically solved together with boundary points at $\psi = \psi_0 = 0$ and $\psi = \psi_{L+1} = 0$. The initial condition is assumed:

$$f^{(n)}(\psi, \tau = 0) = 0, \quad \theta^{(n)}(\psi, \tau = 0) = 0 \tag{19}$$

Time difference semi-implicit scheme for the velocity and temperature profiles is:

$$S\frac{1}{\Delta t}\left(\frac{\partial f^{(n+1)}}{\partial \psi} - \frac{\partial f^{(n)}}{\partial \psi}\right) = \psi^2 \left(\frac{\partial f^{(n)}}{\partial \psi}\right)^2 + 6\psi^2\left(1+\frac{1}{\beta}\right)\frac{\partial f^{(n+1)}}{\partial \psi} - \mathrm{M}^2 \frac{\partial f^{(n+1)}}{\partial \psi} - 2\psi f^{(n)}\left(\frac{\partial f^{(n)}}{\partial \psi}\right) + 6\psi^3\left(1+\frac{1}{\beta}\right)\frac{\partial^2 f^{(n+1)}}{\partial \psi^2} - \psi^2 f^{(n)}\left(\frac{\partial^2 f^{(n)}}{\partial \psi^2}\right) + \psi^4\left(1+\frac{1}{\beta}\right)\frac{\partial^3 f^{(n+1)}}{\partial \psi^3} \tag{20}$$

Table 1. Comparison of $f''(0,\tau)$ with [38, 40] when $S = 1$, $\mathrm{M} = 12$, $\beta \to \infty$

τ	[38]	[40]	Present results
$\tau = 1.5\pi$	11.678656	11.678656	11.6786560
$\tau = 5.5\pi$	11.678707	11.678706	11.678708
$\tau = 9.5\pi$	11.678656	11.678656	11.678656

Table 2. Numerical values of $f''(0,\tau)$ for linear stretching with $S = 0$, $\beta \to \infty$ and $\tau = \pi/2$

M	[44]	[45]	Present results
0	–1.000000	–1.000000	–1.000000
0.5	–1.22474487	–1.224747	–1.2247470
1	–1.41421356	–1.414217	–1.4142172
1.5	–1.58113883	–1.581147	–1.581147
2.0	–1.73205081	–1.732057	–1.7320575

$$S\,\mathrm{Pr}_{eff}\frac{\theta^{(n+1)}-\theta^{(n)}}{\Delta t}=$$
$$=\left[\psi^4\frac{\partial^2\theta^{(n+1)}}{\partial\psi^2}+2\psi^3\frac{\partial\theta^{(n+1)}}{\partial\psi}\right]-$$
$$-\mathrm{Pr}_{eff}\,f^{(n)}\psi^2\frac{\partial\theta^{(n+1)}}{\partial\psi} \tag{21}$$

The important feature of the scheme is that only linear equations at each new time step $(n+1)$ are to be solved. The resulting systems of algebric equations for $f_i^{(n+1)}$ and $\theta_i^{(n+1)}$ at time step $(n+1)$ are solved by using Guassian elimination.

Validation of solution

In order to assess our solution, present outcomes are compared in tab. 1 with available results contributed by noteworthy investigators [38, 40]. It is seen that present results have favorable agreement with these studies. In tab. 2, the present results are reduced for linear stretching as a special case [44, 45]. It is observed that the results for linear stretching are achieved as a limiting case of this study.

Discussion of results

The impacts of involved parameters namely Casson parameter, ratio of oscillation frequency to stretching rate of surface, Hartmann number and effective Prandtl number are discussed on f' and θ. Figures 3(a)-3(c) elaborates the curves of β, S, and M on the time-evolution of f'. The variation of velocity against time for various values of β is depicted in fig. 3(a). We observed that amplitude of the velocity decline periodically by increasing Casson fluid parameter β. Physically, with increase in β the fluid become more viscous and in result the fluid velocity reduces. Figure 3(b) reveals that amplitude corresponding to the flow behavior decays by enhancing S. It is observed that an increase in S results in a pronounced phase shift and decrease in the amplitude of oscillations. Figure 3(c) illustrates the influence of Hartman number with $S = 1$, $\beta = 1$. The investigation predicts that the velocity amplitude decline periodically for larger values of Hartmann number. It is seen that fluid velocity reduces as Hartmann number increases, as expected. It is due to the fact that drag force, also known as Lorentz force is produced when magnetic field is applied to the fluid. This force has the propensity to resist the velocity of fluid in the whole domain.

Figures 4(a)-4(d) displays the influence of dimensionless β on the transverse profile of f' at four different distances $\tau = 8.5\pi$, $\tau = 9\pi$, $\tau = 9.5\pi$, and $\tau = 10\pi$ with fixed $S = 12$ and M = 1.0. In fig. 4(a), the variation of β on f' at fixed time instant $\tau = 8.5\pi$ is shown. The velocity component f' showing a decreasing tendency for higher β. The momentum boundary-layer thickness slightly decreases by increasing β. It is examined that $f' = 1$ at $y = 0$ equating the surface velocity and $f' \to 0$ far away from the surface due to periodic motion of the sheet. For larger values of β, the viscous affects become more dominant which results in decay of velocity. A small oscillation in velocity far away from the surface is attributed due to

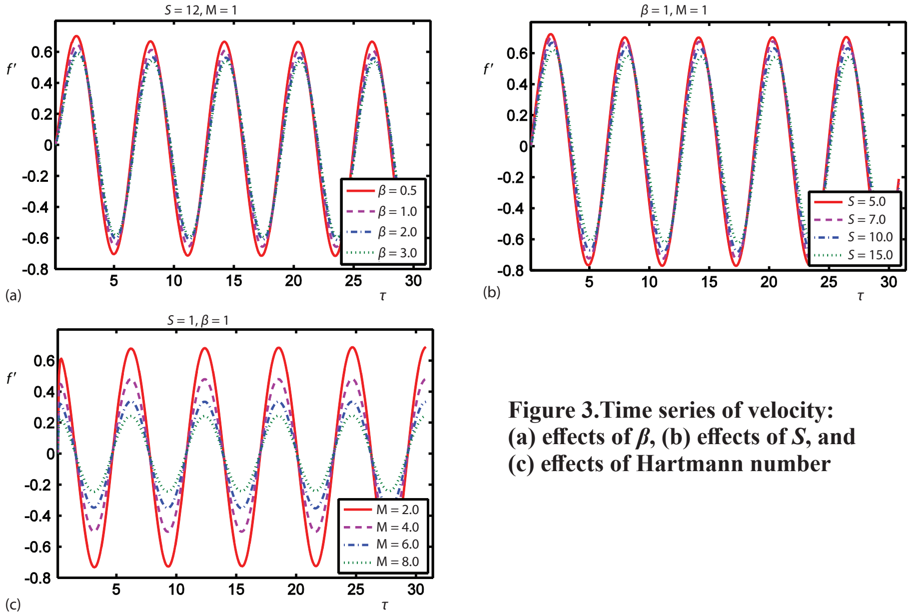

Figure 3.Time series of velocity: (a) effects of *β*, (b) effects of *S*, and (c) effects of Hartmann number

periodic motion of sheet. Figure 4(b) is plotted at time instant $\tau = 9\pi$ which shows that again the velocity decline close to the surface of sheet and after that a slight oscillation is observed before it approaches to zero. The variation of Casson fluid parameter β at time instant $\tau = 9.5\pi$

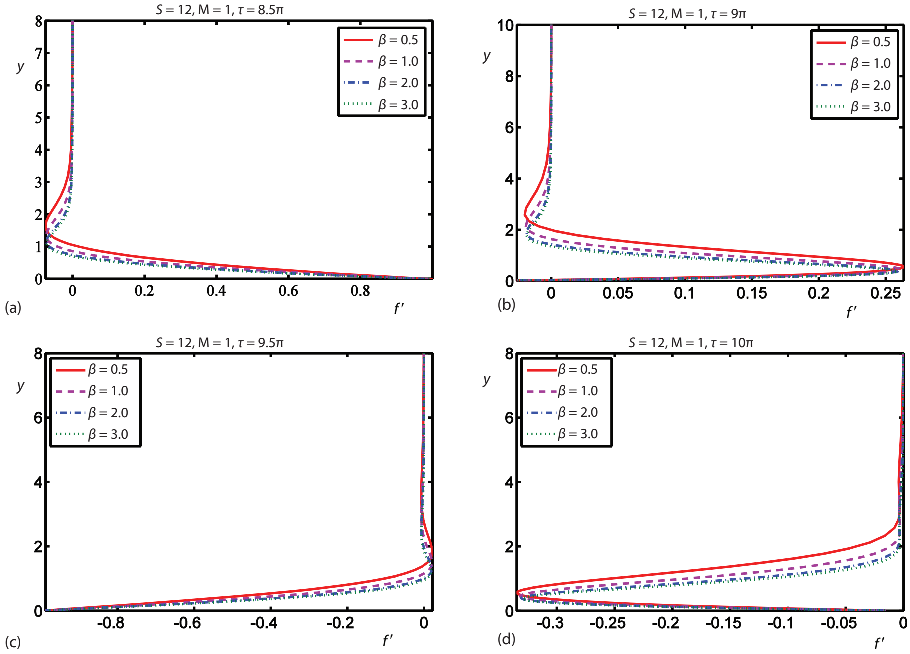

Figure 4. Effects of *β* on velocity

is shown in fig. 4(c). The magnitude of velocity is confined from –1 to zero for larger β. The effects of β at time instant $\tau = 10\pi$ are similar as we observed in fig. 4(d).

The influence of various values of S on the dimensionless velocity component f' at four different distances $\tau = 8.5\pi$, $\tau = 9\pi$, $\tau = 9.5\pi$, and $\tau = 10\pi$ is described in figs. 5(a)-5(d). From fig. 5(a) it is executed that velocity decays by increasing S at time instant $\tau = 8.5\pi$. Figure 5(b) illustrates the effects of S at time instant $\tau = 9\pi$. We see that the velocity f' decline close to the surface of the sheet before approaching to zero. Again, at time instant $\tau = 9.5\pi$, the velocity of the fluid decreases, fig. 5(c). Figure 5(d) reveals that at time instant $\tau = 10\pi$, f' goes to zero at and far from sheet. At same time, we also revealed that the amplitude of back flow enhance by for larger S. The negativity in f' near the surface corresponds to back flow. Figures 6(a)-6(d) demonstrates the effects of Hartmann number on transverse profiles of velocity f' at four different distances by keeping $S = 15$ and $\beta = 1$. Figure 6(a) illustrates the effects of Hartmann number on velocity profile at time instant $\tau = 8.5\pi$. The velocity f' is found to be decreased with increasing Hartmann number. It is noted that the applied magnetic field creates a resistive force known as Lorenz force which decelerates the fluid flow and results in a thinner boundary-layer. This result has prime importance where a reduction in velocity and boundary-layer thickness are required. Now at time instant $\tau = 9\pi$, the velocity oscillates near the surface and finally approaches to zero, fig. 6(b). Figure 6(c) shows the effects of Hartmann number on velocity profile at time instant $\tau = 9.5\pi$. The velocity decreases for higher values of Hartmann number. The effects of Hartmann number on velocity at another time instant $\tau = 10\pi$ are similar to fig. 6(b).

The influence of effective Prandtl number, S, and β on the temperature field θ are illustrated in figs. 7(a)-7(c). In fig. 7(a), the temperature field is observed to be diminished for increasing values of effective Prandtl number since thermal diffusivity decreases for greater values of effective Prandtl number. This decline in temperature inside the boundary-layer by by

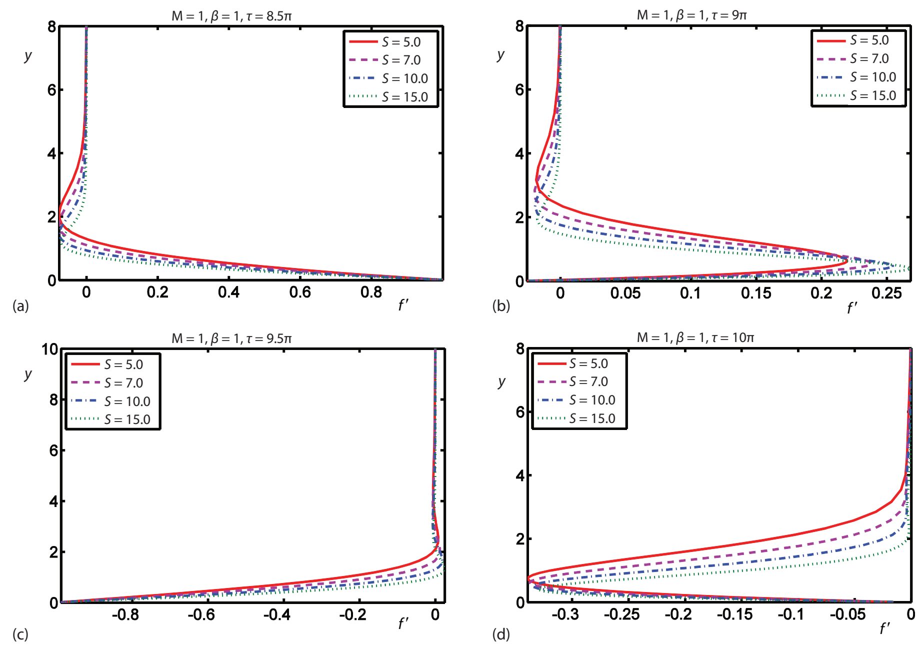

Figure 5. Effects of *S* on velocity

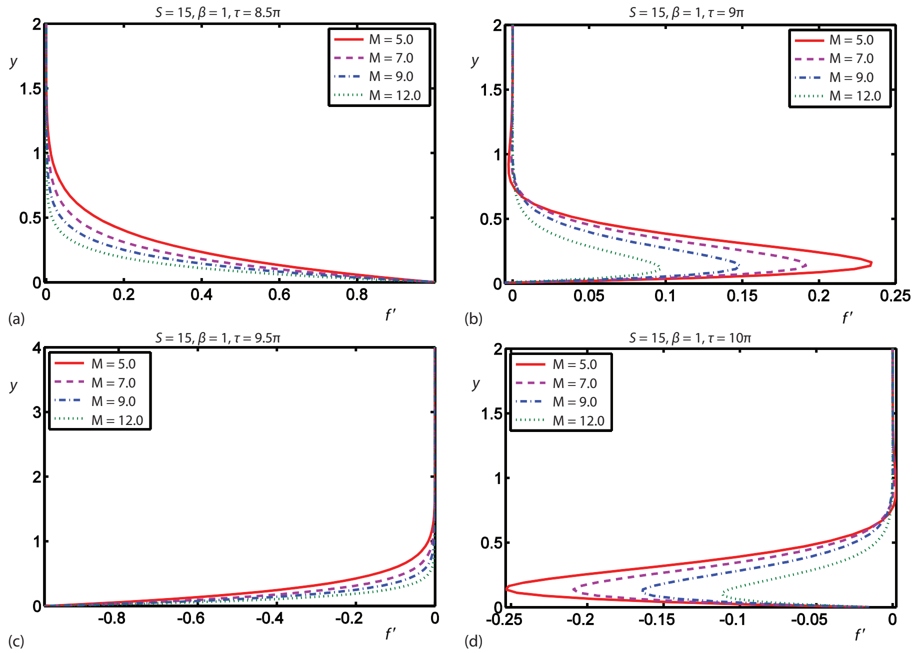

Figure 6. Effects of Hartmann number on velocity

increasing effective Prandtl number is attributed to the fact that effective Prandtl number is directly proportional to Prandtl number and inversely proportional to radiation parameter.

The response of temperature profile, θ, with a range of values of S is depicted in fig. 7(b). The temperature profiles showing a decreasing tendency throughout the region of

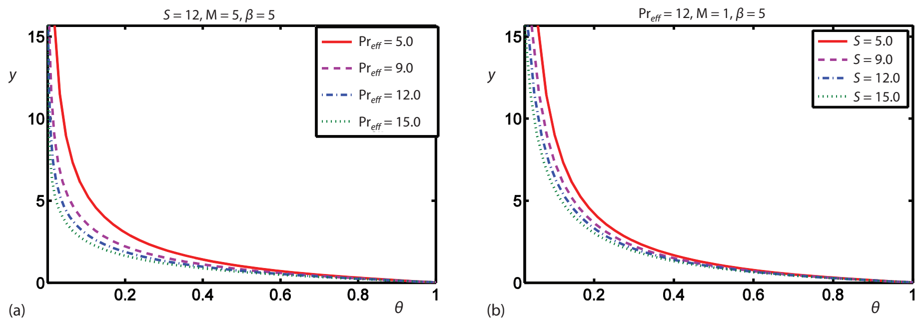

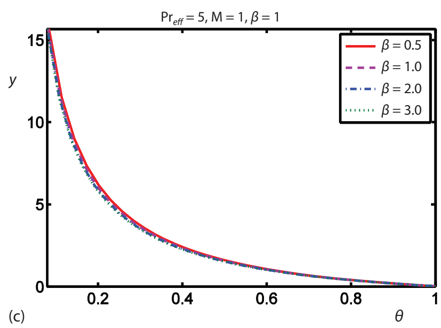

Figure 7. Effects of (a) effective Prandtl number, (b) *S*, (c) *β* on temperature

boundary-layer by increasing S. The effects of Casson fluid parameter, β, on temperature profile are shown in fig. 7(c). It is noted that the temperature profile decreases for by increasing Casson fluid parameter, β. In fact by increasing β, the resistance offered by elasticity of the fluid to its flow increases and as a result of which an increase in temperature inside the thermal boundary-layer is observed. Moreover, a decrease in the relevant thermal boundary-layer thickness is note due to enhancing β. However, this rate of change of heat transfer is minimal as compared with figs. 8(a) and 8(b).

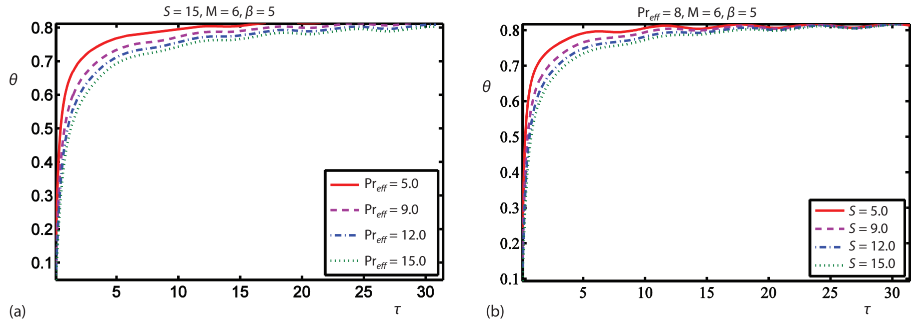

Figure 8. Variation of temperature with time for various values of (a) effective Prandtl number and (b) *S*

The influence of effective Prandtl number and S on θ is shown in figs. 9(a) and 9(b). Figure 9(a) reveals that time-series of the temperature profile decreases by increasing the effective Prandtl number. There exists a small oscillation in the temperature for larger values of effective Prandtl number. Similar observation has been examined in fig. 9(b) *i. e.*, time-series of temperature profile decreases by increasing S. Finally, the variation of effective local Nusselt number with time for various values of effective Prandtl number and S are illustrated in figs. 8(a) and 8(b). It is seen that the effective local Nusselt number increases by enhancing effective Prandtl number and S.

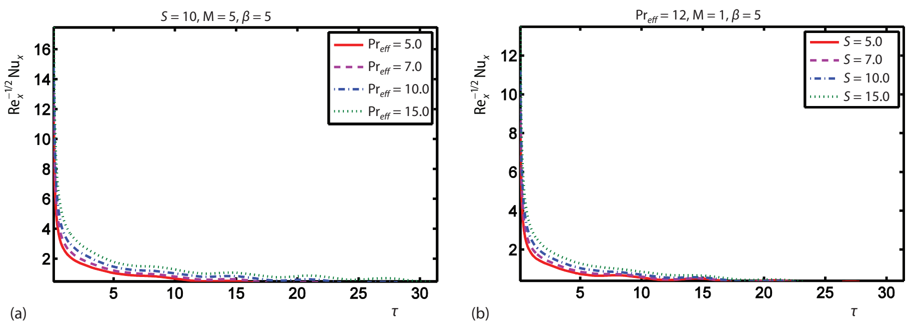

Figure 9.Variation of local Nusselt number with time for various values of (a) effective Prandtl number and (b) *S*

Concluding remarks

We have investigated the numerical problem of MHD radiative Casson liquid over an oscillatory surface through the implementation of implicit finite difference criteria. The influence of emerging parameters is plotted graphically. The investigation predicts that the amplitude of velocity decays periodically for larger values of β, *S,* and Hartann number. Velocity profiles decline for higher values of β, *S,* and Hartmann number. Temperature decreases by increasing effective Prandtl number, *S* and β. The time-series of local Nusselt number increases by enhancing effective Prandtl number and *S*.

Acknowledgment

We are thankful to the anonymous reviewer for his/her useful comments to improve the earlier version of the paper.

Nomenclature

B_0 – strength of applied magnetic field
c_p – specific heat
f' – dimensionless velocity, [–]
k – thermal conductivity
k^* – absorption constant
M – Hartmann number, [$= (\sigma B_0^2/\rho b)^{1/2}$], [–]
N_r – radiative parameter, ($= 16\sigma^* T_\infty^3/3k^*k$)
Nu_x^* – effective local Nusselt number, [–]
Pr – Prandtl number, ($= \mu c_p/k$), [–]
Pr_{eff} – effective Prandtl number, [$= \mathrm{Pr}/(1 + N_r)$], [–]
q_r – heat flux of radiation
Re_x – local Reynolds number, ($= u_w x/\nu$), [–]
T – temperature
T_∞ – ambient temperature
u, v – velocity components

Greek symbols

β – Casson liquid parameter
θ – dimensionless temperature
ρ – liquid density
σ – electrical conductivity
σ^* – Stefan Boltzmann constant
ν – kinematic viscosity

References

[1] Shehzad, S. A., *et al*., Influence of Thermophoresis and Joule Heating on the Radiative Flow of Jeffrey Fluid with Mixed Convection, *Brazilian Journal of Chemical Engineering*, *30* (2013), 4, pp. 897-908
[2] Han, S., *et al*., Coupled Flow and Heat Transfer in Viscoelastic Fluid with Cattaneo-Christov Heat Flux Model, *Applied Mathematics Letters*, *38* (2014), Dec., pp. 87-93
[3] Hayat, T., *et al*., Effect of Joule Heating and Thermal Radiation in Flow of Third Grade Fluid over Radiative Surface, *PLOS One*, *9* (2014), Jan., pp. 3153
[4] Hayat, T., *et al*., Boundary Layer Flow of Walter's B Fluid with Newtonian Heating, *ZeitschriftfürNaturforschung A*, *70* (2015), May, pp. 333-341
[5] Mahdy, A., Chamkha, A. J., Diffusion of Chemically Reactive Species of a Maxwell Fluid Due to an Unsteady Stretching Sheet with Slip Effect, *Thermal Science*, *21* (2017), 6A, pp. 2357-2367
[6] Hussanan, A., *et al*., Unsteady Free Convection Flow of a Micropolar Fluid with Newtonian Heating Closed Form Solution, *Thermal Science*, *21* (2017), 6A, pp. 2313-2326
[7] Abbasi, F. M., *et al*., Analytical Study of Cattaneo-Christov Heat Flux Model for a Boundary Layer Flow of Oldroyd-B Fluid, *Chinese Physics B, 25* (2016), 1, 014701
[8] Krishnamurthy, M. R., *et al*., Effect of Chemical Reaction on MHD Boundary Layer Flow and Melting Heat Transfer of Williamson Nanofluid in Porous Medium, *Engineering Science and Technology, an International Journal, 19* (2016), 1, pp. 53-61
[9] Bhatti, M. M., *et al*., Combine Effects of Magnetohydrodynamics (MHD) and Partial Slip on Peristaltic Blood Flow of Ree-Eyring Fluid with Wall Properties, *Engineering Science and Technology, an International Journal, 19*, (2016), 3, pp. 1497-1502
[10] Walawender, W. P., *et al*., An Approximate Casson Fluid Model for Tube Flow of Blood, *Biorheology*, *12* (1975), 2, pp. 111-124
[11] Hayat, T., *et al*., Soret and Dufour Effects on Magnetohydrodynamic (MHD) Flow of Casson Fluid, *Applied Mathematics and Mechanics (English Edition), 33* (2012), 10, pp. 1301-1312
[12] Bhattacharyya, K., *et al*., Analytic Solution for Magnetohydrodynamic Boundary Layer Flow of Casson Fluid over a Stretching/Shrinking Sheet with Wall Mass Transfer, *Chinese Physics B, 22* (2013), 2, 024702
[13] Mukhopadhyay, S. Diffusion of Chemically Reactive Species in Casson Fluid Flow over an Unsteady Permeable Stretching Surface, *Journal of Hydrodynamics, 25* (2013), 4, pp. 591-598
[14] Shehzad, S. A., *et al*., Effects of Mass Transfer on MHD Flow of Casson Fluid with Chemical Reaction and Suction*, Brazilian Journal of Chemical Engineering, 30* (2013), 1, pp. 187-195

[15] Mukhopadhyay, S., Mandal, I. S., Boundary Layer Flow and Heat Transfer of a Casson Fluid Past a Symmetric Porous Wedge with Surface Heat Flux, *Chinese Physics B, 23* (2014), 4, 044702

[16] Mustafa, M., Khan, J. A., Model for Flow of Casson Nanofluid Past a Non-Linearly Stretching Sheet Considering Magnetic Field Effects, *AIP Advances, 5* (2015), 7, 077148

[17] Shehzad, S. A., *et al.*, Three-dimensional MHD Flow of Casson Fluid in Porous Medium with Heat Generation, *Journal of Applied Fluid Mechanics, 9* (2016), 1, pp. 215-233

[18] Rauf, A., *et al*., Influence of Convective Conditions on Three Dimensional Mixed Convective Hydromagnetic Boundary Layer Flow of Casson Nanofluid, *Journal of Magnetism and Magnetic Materials, 416* (2016), Oct., pp. 200-207

[19] Hussain, T., *et al*., Impact of Magnetic Field in Radiative Flow of Casson Nanofluid with Heat and Mass Fluxes, *Thermal Science*, *22* (2018), 1A, 137-145

[20] Imtiaz, M., *et al*., Mixed Convection Flow of Casson Nanofluid over a Stretching Cylinder with Convective Boundary Conditions, *Advanced Powder Technology, 27* (2016), 5, pp. 2245-2256

[21] Turkyilmazoglu, M., MHD Fluid Flow and Heat Transfer Due to a Shrinking Rotating Disk, *Computers & Fluids, 90* (2014), Feb., pp. 51-56

[22] Zhang, C., *et al*., MHD Flow and Radiation Heat Transfer of Nanofluids in Porous Media with Variable Surface Heat Flux and Chemical Reaction, *Applied Mathematical Modelling, 39* (2015), 1, pp. 165-181

[23] Lin, Y., *et al*., MHD Pseudo-Plastic Nanofluid Unsteady Flow and Heat Transfer in a Finite Thin Film over Stretching Surface with Internal Heat Generation, *International Journal of Heat and Mass Transfer, 84* (2015), May, pp. 903-911

[24] Gireesha, B. J., *et al*., Numerical Solution of Hydromagnetic Boundary Layer Flow and Heat Transfer Past a Stretching Surface Embedded in Non-Darcy Porous Medium with Fluid-Particle Suspension, *Journal of Nigerian Mathematical Society, 34* (2015), 3, pp. 267-285

[25] Heidary, H., *et al*., Magnetic Field Effect on Convective Heat Transfer in Corrugated Flow Channel, *Thermal Science*, *21* (2017), 5, pp. 2105-211

[26] Das, K., *et al*., Thin Film Flow over an Unsteady Stretching Sheet with Thermocapillarity in Presence of Magnetic Field, *Thermal Science*, *21* (2017), 6A, pp. 2369-2378

[27] Turkyilmazoglu, M., Mixed Convection Flow of Magnetohydrodynamic Micropolar Fluid Due to a Porous Heated/Cooled Deformable Plate: Exact Solutions, *International Journal of Heat and Mass Transfer, 106* (2017), Mar., pp. 127-134

[28] Abbas, Z., *et al.*, Hydromagnetic Slip Flow of Nanofluid over a Curved Stretching Surface with Heat Generation and Thermal Radiation, *Journal of Molecular Liquids, 215* (2016), Mar., pp. 756-762

[29] Hayat, T., *et al*., Radiative Flow of Carreau Liquid in Presence of Newtonian Heating and Chemical Reaction, *Results in Physics, 7* (2017), Jan., pp. 715-722

[30] Hayat, T., *et al*., MHD Convective Flow Due to a Curved Surface with Thermal Radiation and Chemical Reaction, *Journal of Molecular Liquids, 225* (2017), Jan., pp. 482-489

[31] Raptis, A., *et al*., Effect of Thermal Radiation on MHD Flow, *Appl. Math.,* 15 *Comput. 153* (2004), 3, pp. 645-649

[32] Pal, D. , Unsteady Convective Boundary Layer Flow and Heat Transfer over a Stretching Surface with Non-Uniform Heat Source/Sink and Thermal Radiation, *International Journal of Computational Methods in Engineering Science and Mechanics, 16* (2015), 3, pp. 170-181

[33] Hayat, T., *et al*., Magnetohydrodynamic Three-Dimensional Flow of Viscoelastic Nanofluid in the Presence of Nonlinear Thermal Radiation, *Journal of Magnetism and Magnetic Materials, 385* (2015), July, pp. 222-229

[34] Sheikhoeslami, M., *et al*., Effect of Thermal Radiation on Magnetohydrodynamics Nanofluid Flow and Heat Transfer by Means of Two Phase Model, *Journal of Magnetism and Magnetic Materials, 374* (2015), Jan., pp. 36-43.

[35] Magyari, E., Pantokratoras, A., Note on the Effect of Thermal Radiation in the Linearized Rosseland Approximation on the Heat Transfer Characteristics of Various Boundary Layer Flows, *Int. Comm. Heat Mass Transfer, 38* (2011), 5, pp. 554-556

[36] Salama, F. A., Effects of Radiation on Convection Heat Transfer of Cu-Water Nanofluid Past a Moving Wedge*, Thermal Science*, *20* (2016), 2, pp. 437-447

[37] Wang, C. Y., Nonlinear Streaming Due to the Oscillatory Stretching of a Sheet in a Viscous, *Acta Mechanica, 72* (1988), 3-4, pp. 261-268

[38] Abbas, Z., *et al*., Hydromagnetic Flow in Viscoelastic Fluid Due to the Oscillatory Stretching Surface, *International Journal of Non-Linear Mechanics, 43* (2008), 8, pp. 783-797

[39] Abbas, Z., *et al*., Slip Effects and Heat Transfer Analysis in a Viscous Fluid over an Oscillatory Stretching Surface, *International Journal of Numerical Methods in Fluids, 59* (2009), 4, pp. 443-458
[40] Zheng, L. C., *et al*., Unsteady Heat and Mass Transfer in MHD Flow over an Oscillatory Stretching Surface with Soret and Dufour Effects, *Acta Mechanica Sinica, 29* (2013), 5, pp. 667-675
[41] Ali, N., *et al*., Hydromagnetic Flow and Heat Transfer of a Jeffrey Fluid over an Oscillatory Stretching Surface, *Z. Naturforsch, 70* (2015), 7, pp. 567-576
[42] Khan, S. U., *et al*., Hydromagnetic Flow and Heat Transfer over a Porous Oscillating Stretching Surface in a Viscoelastic Fluid with Porous Medium, *PLOS ONE, 10* (2015), Dec., pp. 0144299
[43] Ali, N., *et al*., MHD Flow and Heat Transfer of Couple Stress Fluid over an Oscillatory Stretching Sheet with Heat Source/Sink in Porous Medium, *Alexandria Engineering Journal, 55* (2016), 2, pp. 915-924
[44] Turkyilmazoglu, M., The Analytical Solution of Mixed Convection Heat Transfer and Fluid Flow of a MHD Viscoelastic Fluid over a Permeable Stretching Surface, *Int. J. Mech. Sci., 77* (2013), Dec., pp. 263-268
[45] Hayat, T., *et al*., Heat and Mass Transfer for Soret and Dufour's Effect on Mixed Convection Boundary Layer Flow over a Stretching Vertical Surface in a Porous Medium Filled with a Viscoelastic Fluid, *Commun. Nonlinear Sci. Numer. Simul., 15* (2010), 5, pp. 1183-1196

Paper submitted: November 30, 2017
Paper revised: February 21, 2018
Paper accepted: February 22, 2018